Optimized Photoelectrochemical Detection of Essential Drugs bearing Phenolic Groups

Liselotte Neven[1, ‡], Saranya Thiruvottriyur Shanmugam[1, ‡], Vanoushe Rahemi[1], Stanislav Trashin[1], Nick Sleegers[1], Erik N. Carrión[2], Sergiu M. Gorun[2], and Karolien De Wael[1,*]

[1]AXES Research Group, Department of Chemistry, University of Antwerp, Antwerp, Belgium; [2]Department of Chemistry and Biochemistry and the Center for Functional Materials, Seton Hall University, New Jersey 07079, USA

ABSTRACT: The WHO model List of Essential Medicines includes among indispensable medicines antibacterials and pain and migraines relievers. Monitoring their concentration in the environment, while challenging, is important in the context of antibiotic resistance as well as their production of highly toxic compounds via hydrolysis. Traditional detection methods such as HPLC or LC combined with tandem mass spectrometry or UV-Vis spectroscopy are time consuming, have a high cost, require skilled operators and are difficult to adapt for field operations. In contrast, (electrochemical) sensors have elicited interest because of their rapid response, high selectivity and sensitivity as well as potential for on-site detection. Previously, we reported a novel sensor system based on a type II photosensitizer, which combines the advantages of enzymatic sensors (high sensitivity) and photoelectrochemical sensors (easy baseline subtraction). Under red-light illumination, the photosensitizer produces singlet oxygen which oxidizes phenolic compounds present in the sample. The subsequent reduction of the oxidized phenolic compounds at the electrode surface gives rise to a quantifiable photocurrent and leads to the generation of a redox cycle. Herein we report the optimization in terms of pH and applied potential of the photoelectrochemical detection of the hydrolysis product of paracetamol, i.e. 4-aminophenol (4-AP) and two antibacterials, namely cefadroxil (CFD, β-lactam antibiotic) and doxycycline (DXC, tetracycline antibiotic). The optimized conditions resulted in a detection limit of 0.2 µmol L^{-1} for DXC, but in a 10 times higher sensitivity, 20 nmol L^{-1} for CFD. An even higher sensitivity, 7 nmol L^{-1} was noted for 4-AP.

The 2017 World Health Organization (WHO) report, WHO Model List of Essential Medicines compiles a list of medicines which are needed to ensure a basic health system. Antibacterials, such as doxycycline (DXC), are included in this list because they are indispensable medicines. However, due to antibiotic resistance, which is one of the major modern society health problems, the effectiveness of these drugs is often reduced. As a result, the monitoring of antibiotics traces in the environment is important for identifying and eliminating sources of contamination as well as for monitoring antimicrobial consumption and revealing antibiotic resistance patterns.[1, 2]

The misuse as well as the overconsumption of medicines is not limited to antibacterials. For example, the overuse of paracetamol (acetaminophen), which is also included in the WHO model list and commonly used as an antipyretic and analgesic, leads to an accumulation of its toxic, hydrolytic product 4-aminophenol (4-AP) with liver and kidney impairment as a result.[3, 4] Notably, 4-AP is produced as an intermediate in the synthesis of paracetamol.[5] So, its quantification is useful for environmental monitoring, quality control purposes and detection of paracetamol use.

The detection of 4-AP in environmental samples, as well as that of DXC, is challenging since the analytes could be present in very low concentrations (ng L^{-1}) in complex matrices.[6] Still, a considerable effort has been spent to detect these compounds. Conventional methods include liquid chromatography (LC), high performance liquid chromatography (HPLC) combined with tandem mass spectrometry[6-8] or UV-Vis detection[6, 9, 10]. Despite their high accuracy and their ability to handle complex samples[8, 11], these methods require expensive equipments, skilled personnel, are time-consuming, need most of the time a pre-concentration step[10, 12] and, importantly, remain laboratory methods. Thus, rapid and easy-to-use detection strategies are of great interest, including for on-site-monitoring.

(Bio)sensors-based detection has emerged as a valuable alternative or complementary methodology to traditional ones.[12-19] Biosensors could be integrated with various detection techniques, such as surface plasmon resonance, colorimetry, fluorescence, (electro)chemiluminescence and electrochemistry. The specific combination of biosensors with (photo)electrochemical detection strategies provides several advantages, such as simplicity of the instrumentation and detection strategy, portability, rapid response, low cost, high sensitivity and the need for only a small amount of sample.[20-23] It has led, consequently, to a wide application range in the detection of chemical analytes.

The idea of using light combined with electrochemical detection for sensors has attracted much attention.[23-26] In these sensors the response is only triggered when their surface is illuminated, thus allowing an easy dark baseline subtraction.[27] We reported recently a novel, bioinspired approach that takes advantage of an enzymatic sensor (amplification through electrocatalytic redox cycling) with photoelectrochemical detection.[28] We used a robust, fluorinated Zn phthalocyanine com-

plex as photosensitizer type II, which generates aerobically singlet oxygen under illumination,[29-31] to be used as an oxidizing agent, unlike the enzymatic sensor that uses hydrogen peroxide for the same purpose. The produced singlet oxygen oxidizes all phenolic compounds present in the sample; its subsequent reduction completes the electrocatalytic redox cycle while the measured photocurrent reveals the total concentration of phenols present in the solution. This photoelectrochemical detection strategy affords an improved sensitivity and a low detection limit (20 nmol L^{-1} for amoxicillin). A profound analysis and optimization of the factors that influence the photoelectrochemical response, however, has not yet been performed.

We report herein an evaluation of the effects of variation of pH, applied potential and structural features of analyzed phenolic compound on the photoelectrochemical response. The chosen compounds, Figure 1, include 4-AP a mono, para amino substituted phenolic compound and DXC, an antibiotic with a phenolic ring as part of a tetracyclic structure. Two related molecules, namely benzyl-substituted amino β-lactam antibiotics have been used to provide insights in the role of the phenolic group: cefadroxil (CFD) (C) and cephalexin (CFL) (D), which exhibit and lack an aromatic OH group (phenolic group), respectively. Amoxicillin (E) and CFD (C), which contain identical phenolic moieties, but differ in their overall structures, are also compared.

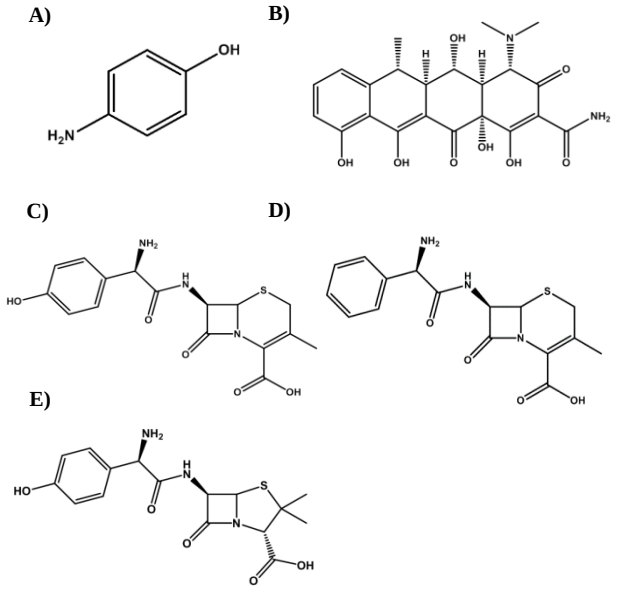

Figure 1. Molecular structures of 4-AP (A), DXC (B), CFD (C), CFL (D) and amoxicillin (E).

EXPERIMENTAL

Reagents. The perfluorophthalocyanine Zn complex (F_{64}PcZn) was synthesized and immobilized on a titania P25 matrix (F_{64}PcZn|TiO_2).[32] Powders of F_{64}PcZn|TiO_2 2-3 wt% loading were used in all experiments, if not mentioned otherwise. KH_2PO_4 and KCl, used for making phosphate buffer solution, were purchased from Sigma-Aldrich (Belgium).

DXC hyclate, 98 % purity and CFD of > 95% purity were purchased from Across Organics. CFL of > 98 % purity was obtained from TCI chemicals. 4-AP of purity > 98 % was purchased from Sigma-Aldrich. The antibiotics were dissolved in ultrapure water while 4-AP was dissolved in absolute ethanol. A stock solution of 4-AP, heat and light sensitive was stored in an ice box in the absence of light.

Equipment. Electrochemical measurements were carried out using a μAutolab III (Metrohm Autolab) instrument. As illumination source, a diode laser (Roithner Lasertechnik) operating at 655 nm was set to a power of 30 mW. The laser power was turned on and off at certain time intervals. The first illumination was used to adjust the laser beam focus to fully cover the working electrode surface by adjusting the distance of the laser source from the working electrode surface. This distance was fixed for all experiments.

The scanning electron microscopy (SEM) image is taken by the FEI Quanta 250 (Thermo Fisher Scientific) at 30 kV.

Screen-printed Electrodes. Graphite screen-printed electrodes (SPE) were purchased from DropSens. A 5 μL droplet of an aqueous suspension of F_{64}PcZn|TiO_2 was deposited on the working electrode surface and the electrode was left to dry overnight producing a F_{64}PcZn|TiO_2-coated SPE. The amount of F_{64}PcZn|TiO_2 deposited on the electrode was optimized based on reproducibility and on maximizing the value of the photocurrent response.

For linear sweep voltammetric measurements, the SPEs were treated with 0.1 mol L^{-1} HNO_3 prior to the photosensitizer deposition. This step was performed to avoid the distortion of voltammograms in the optimum potential region due to silver reduction at the working electrode.

Electrochemical measurements. The electrochemical measurements were conducted in droplets of 80 μL. The measuring buffer consisted of 0.02 mol L^{-1} KH_2PO_4 dissolved in ultrapure water. The pH of the buffer solutions was adjusted to the desired value with KOH and H_3PO_4 solutions. Furthermore, 0.1 mol L^{-1} KCl, acting as supporting electrolyte, was added to the buffer solutions. Buffers of different pH values were used in the experiments. For pH 10 measurements, 0.1 mol L^{-1} KCl and 0.02 mol L^{-1} H_3BO_4 buffer was used. A saturated calomel electrode was used to determine the potential of the Ag pseudo-reference electrode of the SPEs. This reference electrode had a potential of approximately +0.05 V vs SCE in the measuring buffer. The values of the potential are given versus the Ag pseudo-reference electrode of the SPE, if not mentioned otherwise.

RESULTS AND DISCUSSION

Optimization of photosensitizer loading on electrodes. The dependence of the photoelectrochemical response on the amount of the photosensitizer deposited on the surface of the electrode was examined, Figure 2. Drops containing four different concentrations of F_{64}PcZn|TiO_2, namely 2.5, 5 10 and 20 mg mL^{-1} were casted on the surface of the electrodes. The electrodes obtained using the 10 mg mL^{-1} concentration showed practically good coverage on the working surface and good reproducibility compared to the 20 mg mL^{-1} concentration case. Noting a slightly lower, but comparably high photocurrent response relative to 20 mg mL^{-1} concentration, the 10 mg mL^{-1} concentration was selected as the optimum for further studies based on its good reproducibility**.** The SEM image (Figure 3) of the 10 mg mL^{-1} coating show that the supported photosensitizer is distributed over the whole working electrode producing a rough surface. As a consequence, the active sur-

face area available for illumination is increased leading to a higher amount of produced singlet oxygen and thus, increasing the oxidation probability of the phenolic compound.

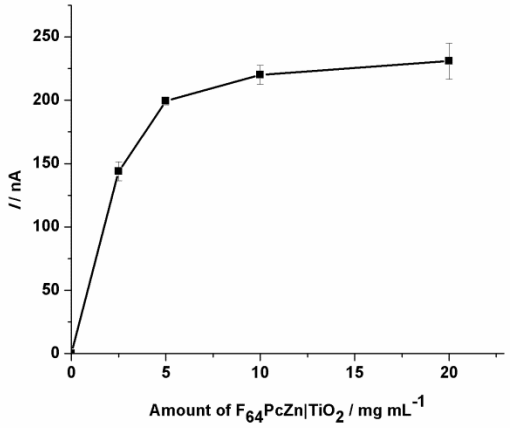

Figure 2. Plot of the effect of variable $F_{64}PcZn|TiO_2$ loadings on the working electrode response. 5 µL aqueous drops of different concentrations were drop casted on the working surface.

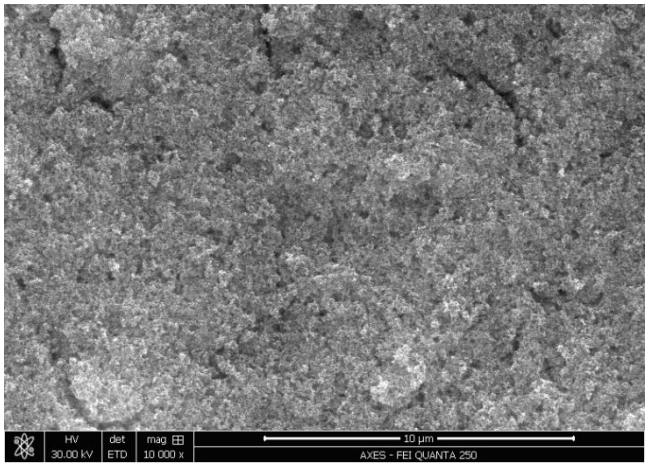

Figure 3. SEM image of coated $F_{64}PcZn|TiO_2$ working electrode of SPE. Coating is made from a 5 µL drop of 10 mg mL^{-1} aqueous solution.

Detection of phenolic analytes. To understand the photoelectrochemical behaviour of the analytes at different potentials, linear sweep voltammograms were recorded. A slow scan rate was applied to ensure the appearance of a photocurrent during a small potential region and, thereby making it easier to identify at which potential the photocatalysis is initiated.

The linear sweep voltammograms of CFD, DXC and 4-AP are shown in Figure 4. For all molecules, a clear difference between the blank current (phosphate buffer, pH 7, red continuous line) and the curve of the phenolic compound (black dotted line) is observed.

The photocurrent for the blanks, which is smaller compared with the photocurrent for the phenolic compounds at all times is attributed to the reduction of the formed $^1O_2$ at the electrode surface[28]. In contrast, in the presence of a phenolic compound,

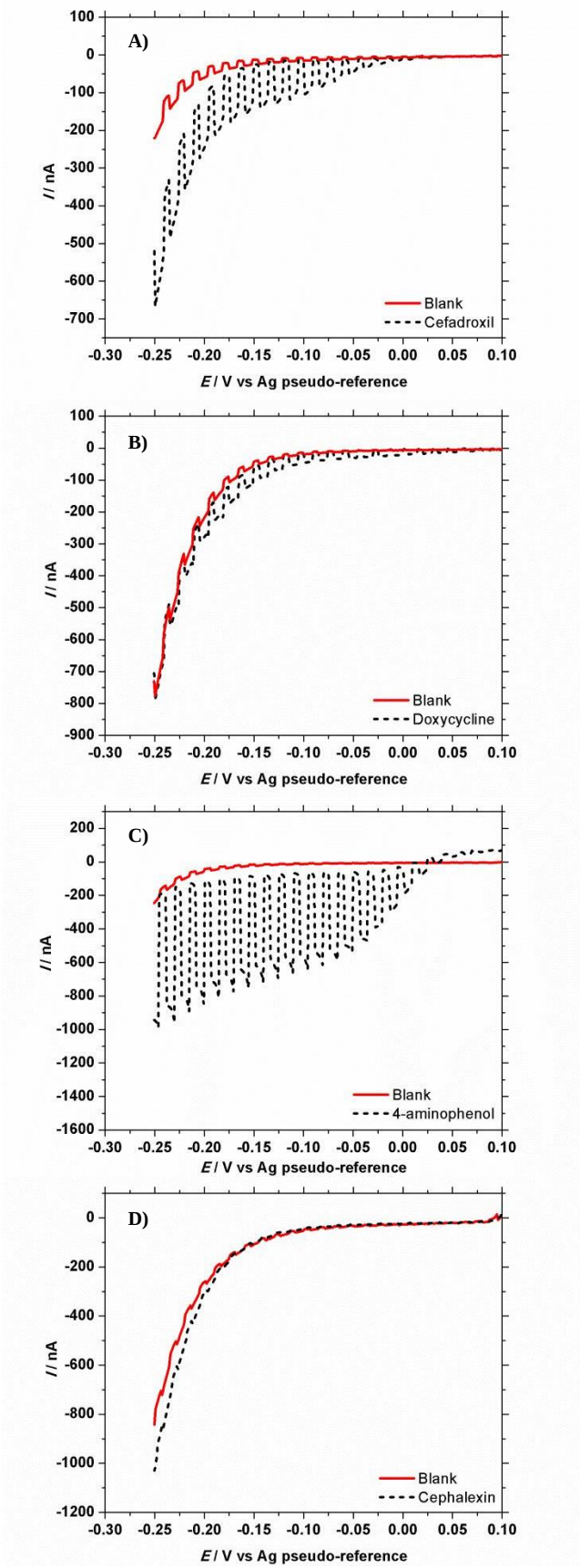

Figure 4. Linear Sweep Voltammograms of 10 µmol L^{-1} CFD (A), DXC (B), 4-AP (C) and CFL (D) (dotted line) recorded at 0.25 mV s^{-1} scan rate and 1 mV step potential are presented. The laser was programmed to switch on and off at 30 s intervals. The blank is the phosphate buffer at pH 7 (red continuous line).

a noticeably larger signal is obtained when a sufficiently negative potential is applied. This is due to the efficient reduction of the oxidized phenolic compounds in the electrocatalytic redox cycle.

The proof that the phenolic moiety is responsible for the electrocatalytic redox cycle was obtained by comparing the linear sweep voltammograms of CFD and CFL, Figure 4, A and D. The structures of CFD and CFL, Figure 1 C and D are identical with the exception of the presence of a hydroxyl group in CFD. Unlike the case of CFD, no clear difference between the photocurrent in the presence and absence of CFL is observed. CFL does not produce a response under illumination, supporting the notion that the phenolic moiety of the side chain and not the cephalosporins' core structure causes the appearance of a photocurrent. This conclusion is further confirmed by the photocurrent response of 4-AP, a molecule which contains only a phenolic moiety and a primary amine.

Interestingly, the redox cycle of DXC is initiated at more positive potentials than for CFD (Figure 4, A and B). From a potential of 0.05 V vs. Ag pseudo-reference, a small photocurrent is differentiated from the blank curve. Therefore, it seems that the oxidized DXC molecules are more easily reduced than the oxidized CFD molecules at the electrode surface. The photocurrent response of 4-AP (Figure 4, C) can be observed from 0.08 V vs. Ag pseudo-reference. Its amplitude is also comparatively higher due to the faster kinetics of singlet oxygen mediated redox cycle at pH 7.[33]

Optimization of measurement parameters. In order to implement an efficient detection strategy, the optimization of measurement parameters is crucial. Thus, both the applied potential and the pH of the measuring buffer were optimized. The blank linear sweep voltammetric curves (Figure 4, black curves) reveal that from a certain potential, there is a contribution from the blank buffer to the photocurrent response. This buffer photocurrent contribution was considered as noise, while the photocurrent obtained in the presence of an analyte as signal. Their ratio, R_{ls}, is the experimental signal-to-noise ratio. The applied potential with maximum R_{ls} was chosen as the optimum potential. To determine this potential, an optimum potential region was selected first based on the linear sweep voltammograms of the phenolic compounds (Figure 4).

For CFD, (Figure 4, A) this optimum potential region is from -0.15 V to -0.1 V. At potentials more negative than -0.15 V, a higher contribution of the measuring buffer to the photocurrent response was observed, resulting in a lower signal-to-noise ratio, while at potentials more positive than -0.1 V, a noticeable lower photocurrent response of CFD is observed. For DXC, the optimum potential region is shifted towards more positive values: -0.125 V to -0.075 V; for 4-AP, the optimum potential region lies between -0.15 V to -0.05 V with a relative high R_{ls}.

Since the linear sweep voltammograms only give an indication where the optimum potential lies (due to the switching on and off of the laser which is necessary to observe the photocurrent response and the baseline curve, respectively) amperometric measurements were performed to accurately determine the photocurrent of the phenolic analytes and the measuring buffer. Similar to linear sweep experiments, the optimization criterion chosen was based on the ratio, termed R_{am} of the photocurrent response of the analyte to the photocurrent response of the measuring buffer. Thus, by varying the applied potential and the pH of the measuring buffer, the optimum applied potential and pH can be determined. Plots of R_{am} vs. pH are shown in Figure 5.

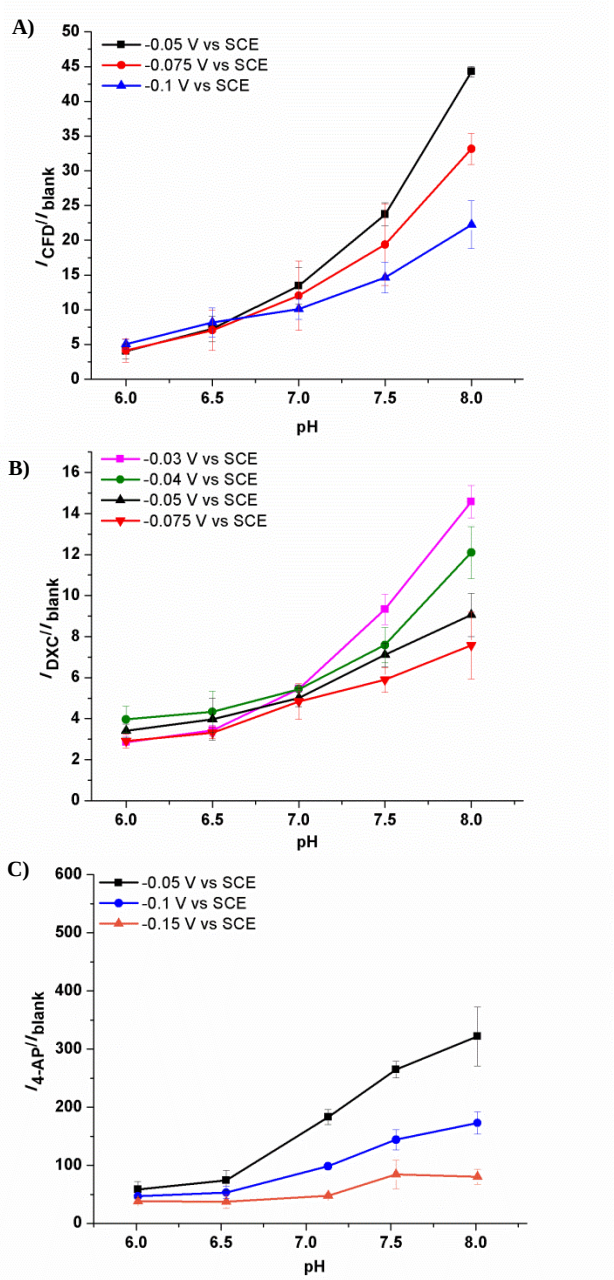

Figure 5. Plots of R_{am} the ratio of the photocurrent response of the phenolic compound to that of the blank, function of the pH of the measuring buffer, 0.1 mol L^{-1} KCl and 0.02 mol L^{-1} KH_2PO_4. A) CFD, B) DXC and C) 4-AP.

Several pH values between 6 and 8 were considered. An optimum pH of 8 and applied potential of -0.05 V vs. SCE for CFD (R_{am} = 44.3 ± 0.8) and 4-AP (R_{am} = 321.7 ± 51), and -0.03 V vs. SCE for DXC (R_{am} = 14.6 ± 0.8) were determined. Although the R_{am} at pH 8 for 4-AP is the highest, the error bars are too large indicating reduced reproducibility. This may be explained by the fact that 4-AP is sensitive to the environment and deteriorates under the influence of air and light. The kinetics of 4-AP autoxidation in aqueous solutions is also different for pH 8 and above.[34] Hence, for further experiments pH 7.5 (R_{am} = 264.6 ± 14) was chosen as the optimum value.

As the pH of the measuring buffer is increased, higher R_{am} values are observed. Several effects can cause this increase. Firstly, a decrease in the photoresponse of the measuring buffer is observed in function of the pH (Figure 6). The potential threshold at which the contribution of the measuring buffer changes from an oxidative current to a reductive photocurrent (indicated by the arrows), shifts towards more negative potentials as the pH is increased. As a result, the reductive photocurrent is smaller when the applied potential is closer to this threshold value.

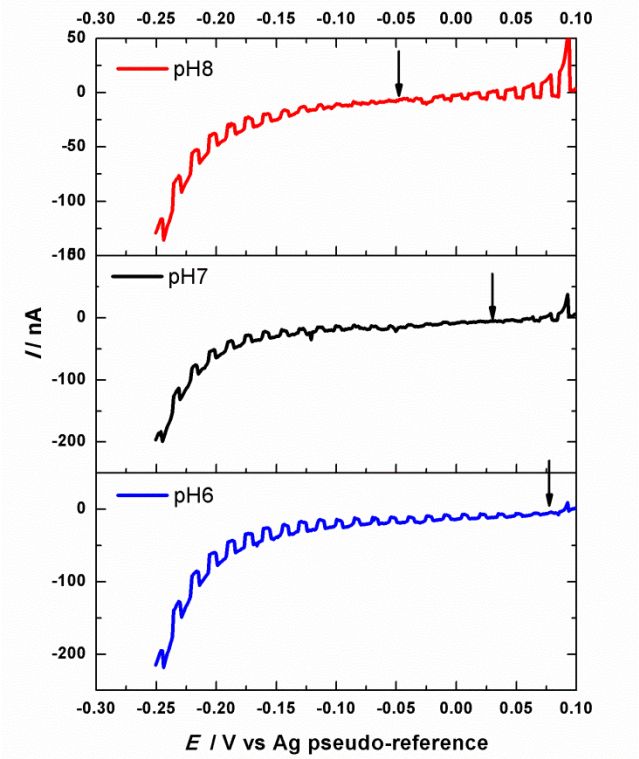

Figure 6. Linear Sweep Voltammograms of 0.1 mol L^{-1} KCl and 0.02 mol L^{-1} KH_2PO_4 at pH 6, 7 and 8. The arrows indicate the potential range at which the oxidizing current changes to a reductive one.

Secondly, if phenol is used as a model for these compounds, two competing pathways can explain the increasing photocurrent response function of the pH. In the first pathway phenols are oxidized by singlet oxygen (pathway 1a: oxidation of the neutral species). This oxidation rate increases function of the pH.[35] Moreover, the deprotonation of the hydroxyl group can lead to a 100 times higher oxidation rate (pathway 1b: oxidation of the phenolate ion).[36] However, a second pathway, which does not involve singlet oxygen competes with the first one. According to this pathway, there is an electron exchange between the excited photosensitizer and the phenolate ion leading to a reduced photosensitizer species and a phenoxyl radical.[35] Since the photochemically reduction of F_{64}PcZn was already observed in ethanol in the absence of oxygen and without the need of additional reagents,[37] this pathway seems likely to occur.

For CFD and DXC (Figure 5 A and B), the curves appear similar: there is a bigger increase of the value of R_{am} on moving from acidic to alkaline conditions. In acidic media pathway 1a contributes largely to this increase together with the decrease of the photocurrent response of the measuring buffer. However, towards more alkaline conditions, increasing amounts of phenolate ions are present leading to a larger contribution of pathways 1b and 2. Although the amount of phenolate ions in the case of CFD is small (pKa: 9.6),[38] for DXC at pH 8, the majority of the species will be in the form of the phenolate ion (pKa: 7.7).[39, 40]

However, the curve for 4-AP (Figure 5 C) does not follow the same pattern as the curves for CFD and DXC. The increase is not as much as that observed for CFD and DXC, presumably due the higher pKa value of the hydroxyl group,10.4,[41] leading to a reduced contribution of pathway 1b in the studied pH range.

pH-dependent photocurrent variation shapes. As the pH of the measuring buffer is increased, the shape of the observed photocurrent of DXC changed accordingly, Figure 7. It is postulated that this change correlates with the pKa value of the phenolic moiety, which for DXC is 7.7.[39, 40] When the pH of the measuring buffer is lower than the pKa value of the phenolic group, e.g. 6, the photocurrent corresponds to shape A. From the start of the illumination of the electrode surface, an increasing photocurrent is observed followed by its stabilization in time. In contrast, when the pH of the measuring buffer is above this pKa, e.g. 8, the photocurrent is characterised by a spike which then decreases to a steady-state value function of time (shape B). There is no difference in the time needed for the stabilization of the photocurrent for the two different shapes.

The spike in shape B increases even more as higher negative potentials are applied at pH 8. At pH 7 (< pKa of DXC), when potentials of -0.075 V and -0.1 V are applied, the shape of the photocurrent is beginning to form shape B while at a potential of -0.05 V shape A is observed. This incipient formation of shape B can be explained by the presence of small amount of ionized DXC species. Moreover, shape B is not formed at pH 6 when the applied potential is increased. Since the oxidation of phenols increases function of the pH and the reduction of the oxidized species increases with more negative applied potentials, it can be concluded that the oxidation as well as the reduction kinetics are the critical parameters for the full generation of shape B.

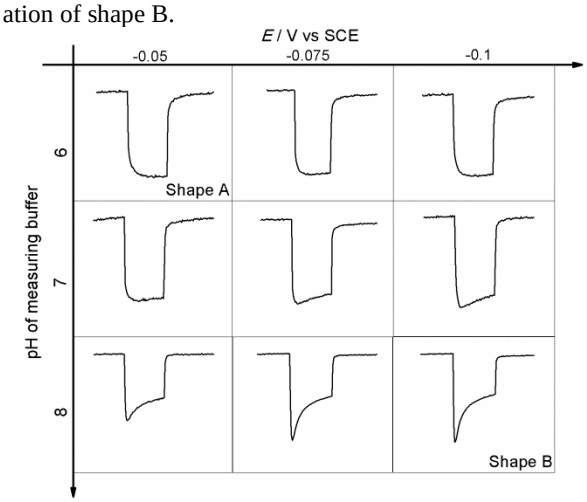

Figure 7. The shape of the photocurrent of DXC (pKa 7.7) as a function of pH of the measuring buffer and the applied potential (the current is not in scale) with indication of shape A and B.

For CFD (Figure 8 A) a similar change in the photocurrent is not observed in the range of investigated buffer pH values since the pKa value of the phenolic group is higher, namely

9.6.[38] To observe a change in the shape of the photocurrent, more alkaline buffer solutions were used. Indeed, at pH 10, the photocurrent shape approached type B, but it was not as clearly defined as that for DXCs due to the lower stability of the antibiotic at this alkaline pH.[42] Measurements at higher pH values could not be performed due to instability of photocurrent responses over several illuminations levels and, possibly, degradation of the antibiotic. At pH 8, shape A was observed.

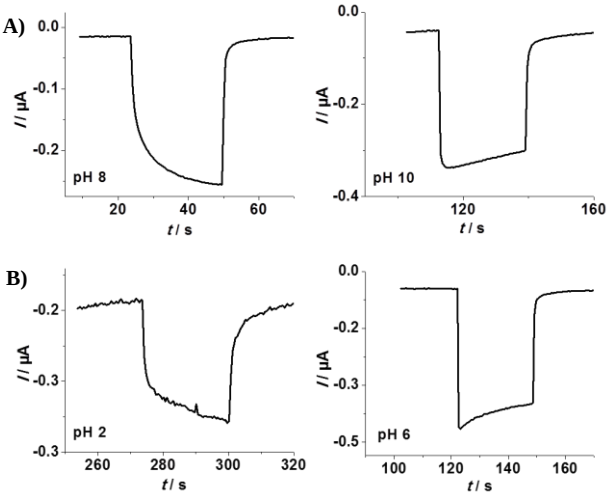

Figure 8. Shape of the photocurrent variations for CFD (A) and 4-AP (B) function of the pH of the measuring buffer.

Interestingly, in the case of 4-AP (Figure 8 B) the change of the shape of the photocurrent occurs between pH 2 and pH 6. It is postulated that this change is not caused by the deprotonation of the hydroxyl group, which has a pKa of 10.4 but by the deprotonation of the positively charged amine-group, pKa 5.4.[41]

At optimum conditions both DXC and 4-AP produce shape B, while CFD produces shape A.

The understanding of the origins of the photocurrent shapes is important when analysing unknown samples since insights on the pKa values of compounds of interest could be obtained from the shapes - pH dependency.

Limits of detection. The limit of detection (LOD) for the phenolic analytes was determined by the ratio of three times the standard deviation of the blank over the gradient of the calibration curve. For each of the analytes, a calibration curve was established, Figure 9.

A two times lower LOD for CFD is determined when 3 wt% $F_{64}PcZn|TiO_2$ coatings are used instead of 2 wt% $F_{64}PcZn|TiO_2$. For this reason, calibration curve are constructed based on measurements with 3 wt% $F_{64}PcZn|TiO_2$.

The LOD value for CFD is 20 nmol L^{-1} with a sensitivity of the sensor of 0.24 A M^{-1} cm^{-2} using the optimized conditions. This value is in the same range as the previously determined LOD of amoxicillin, which is also a β-lactam antibiotic with a phenolic group.[28] For DXC a LOD of 0.2 µmol L^{-1} was determined. This LOD is 10 times higher than the LOD of CFD; a decrease in sensitivity was also noted for DXC, namely 0.024 A M^{-1} cm^{-2}. In contrast, 4-AP has the lowest LOD, 7 nmol L^{-1} with a high sensitivity of 0.21 A M^{-1} cm^{-2}, the relative parameters being also evidenced by the corresponding linear sweep voltammograms. These obtained LODs demonstrate the high sensitivity of the sensor towards 4-AP and CFD when compared with literature LOD values.[17, 18, 43]

It should be understood that, for the reported photoelectrochemical sensor, multiple parameters can influence the amplitude of the photocurrent and cause sensitivity differences. The kinetics of electrochemical reduction at the electrode surface, diffusion or kinetics of oxidation by singlet oxygen are examples of these parameters.

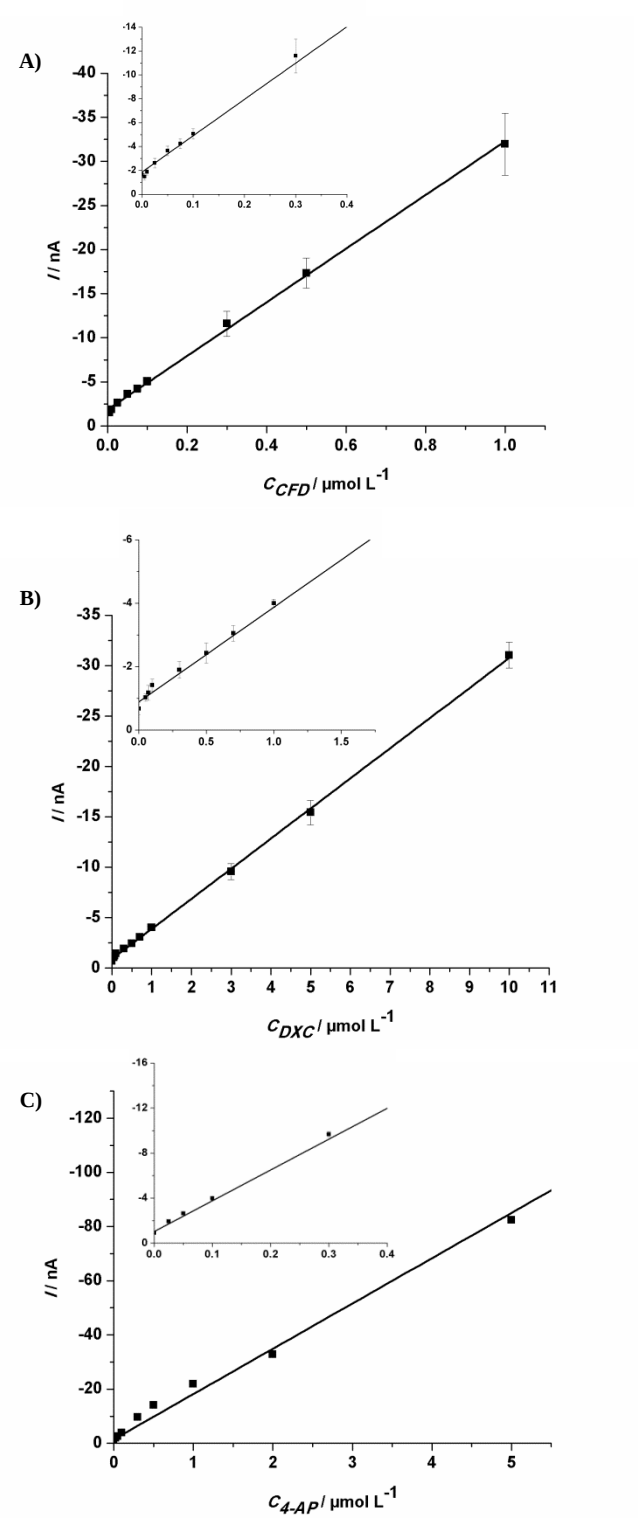

Figure 9. Calibration plots of A) CFD, B) DXC and C) 4-AP.

Although an optimum applied potential was determined, the rate of the electrochemical reduction at the electrode surface

can differ for the examined compounds. While the photocurrent response appeared at relatively less negative potentials for DXC than for CFD, it is possible that the rate of reduction for DXC is slower than that for CFD, thus explaining at least in part the lower sensitivity. The determination of the formed oxidation products could provide insights into this matter, most likely linked to structural differences. In addition, the rate of oxidation by singlet oxy gen can contribute to sensitivity differences. Tratnyek et al.[36] already showed that the reaction rate of phenols with singlet oxygen is influenced by its substituents. It was observed that electron withdrawing substituents decrease the reaction rate of oxidation by singlet oxygen since these substituents make the phenolic ring electron poor. As a result, these compounds are less susceptible to oxidation via electron loss. DXC contains an electron withdrawing group (acetyl function group attached to the ring) which can be responsible for the lower photoresponse due to diminished reaction rates and, accordingly, the higher detection limit. Moreover, its phenyl group shares, also, a carbon-carbon bond with the adjacent ring. In other words, its oxidation by singlet oxygen can be more challenging than in the case of CFD, which has a free phenol ring and, therefore, more positions available for this oxidation process.

The same reasoning can be made for 4-AP. The amino group can function as an electron donating group making the ring more susceptible to oxidation via electron loss and thus explaining its low detection limit compared with CFD. Furthermore, due to the structural complexity of DXC and CFD, it is not unlikely that other regions in the structure might be oxidized by singlet oxygen.

CONCLUSIONS

The photoelectrochemical detection of CFD, DXC and 4-AP was optimized in terms pH of the measuring buffer and applied potential. The photocurrent response increased function of pH and an optimum pH of 8 was determined for the detection of CFD and DXC, and 7.5 for 4-AP. A slightly less negative potential relative to that of CFD was determined to be optimum for the detection of DXC, a finding attributed to the fact that the redox cycle of DXC is initiated at less negative potentials than for CFD. A 10 times higher detection limit for DXC relative to that for CFD was observed, presumably due to structurally-related slower oxidation by singlet oxygen and reduction kinetics for DXC. Although the detection of CFD and 4-AP gave satisfactory detection limits, the detection of DXC should further be optimized. While the reported singlet oxygen electrosensing strategy proved valuable in the detection of phenolic compounds, the differences in sensitivity and an in-depth understanding of the singlet oxygen chemistry influence on sensor parameter might benefit from a complete elucidation of the reduced and oxidized species that participate in the redox chemistry.

AUTHOR INFORMATION

Corresponding Author

* E-mail: karolien.dewael@uantwerpen.be

Author Contributions

The manuscript was written through contributions of all authors.
‡Shared first authorship.

ACKNOWLEDGMENT

FWO (file number: 1S09518N, 1S3765817N and 12T4219N) is acknowledged for financial support. The Center for Functional Materials of Seton Hall University is thanked for support (SMG and ENC). Joren Van Loon is thanked for the graphical abstract. This research was supported by the medium scale research infrastructure funding-Hercules funding (SEM).

REFERENCES

1. Weist, K.; Muller, A.; Hoxha, A.; Vlahović-Palčevski, V.; Elias, C.; Monnet, D.; Heuer, O. *Surveillance of antimicrobial consumption in Europe: 2013-2014*; ECDC: 2018.
2. O'Neill, J. *Tackling Drug-Resistant Infections Globally: Final Report And Recommendations*; 2016.
3. Menon, S.; Jesny, S.; Kumar, K. G. A voltammetric sensor for acetaminophen based on electropolymerized-molecularly imprinted poly(o-aminophenol) modified gold electrode. *Talanta* **2018,** *179*, 668-675.
4. Yin, H. S.; Shang, K.; Meng, X. M.; Ai, S. Y. Voltammetric sensing of paracetamol, dopamine and 4-aminophenol at a glassy carbon electrode coated with gold nanoparticles and an organophillic layered double hydroxide. *Microchim Acta* **2011,** *175* (1-2), 39-46.
5. Feng, X. W.; Zhang, Q. H.; Cong, P. S.; Zhu, Z. L. Determination of the paracetamol degradation process with online UV spectroscopic and multivariate curve resolution-alternating least squares methods: comparative validation by HPLC. *Anal Methods-Uk* **2013,** *5* (19), 5286-5293.
6. Seifrtova, M.; Novakova, L.; Lino, C.; Pena, A.; Solich, P. An overview of analytical methodologies for the determination of antibiotics in environmental waters. *Anal Chim Acta* **2009,** *649* (2), 158-179.
7. Colin, P.; De Bock, L.; T'jollyn, H.; Boussery, K.; Van Bocxlaer, J. Development and validation of a fast and uniform approach to quantify beta-lactam antibiotics in human plasma by solid phase extraction-liquid chromatography-electrospray-tandem mass spectrometry. *Talanta* **2013,** *103*, 285-293.
8. Bogialli, S.; Di Corcia, A. Recent applications of liquid chromatography-mass spectrometry to residue analysis of antimicrobials in food of animal origin. *Anal Bioanal Chem* **2009,** *395* (4), 947-966.
9. Abdelaleem, E. A.; Abdelwahab, N. S. Validated stability indicating RP-HPLC method for determination of paracetamol, methocarbamol and their related substances. *Anal Methods-Uk* **2013,** *5* (2), 541-545.
10. Benito-Pena, E.; Partal-Rodera, A. I.; Leon-Gonzalez, M. E.; Moreno-Bondi, M. C. Evaluation of mixed mode solid phase extraction cartridges for the preconcentration of beta-lactam antibiotics in wastewater using liquid chromatography with UV-DAD detection. *Anal Chim Acta* **2006,** *556* (2), 415-422.
11. Gros, M.; Petrovic, M.; Barcelo, D. Tracing Pharmaceutical Residues of Different Therapeutic Classes in Environmental Waters by Using Liquid Chromatography/Quadrupole-Linear Ion Trap Mass Spectrometry and Automated Library Searching. *Anal Chem* **2009,** *81* (3), 898-912.
12. Lan, L. Y.; Yao, Y.; Ping, J. F.; Ying, Y. B. Recent advances in nanomaterial-based biosensors for antibiotics detection. *Biosens Bioelectron* **2017,** *91*, 504-514.
13. Chen, X. M.; Zhao, L. M.; Tian, X. T.; Lian, S.; Huang, Z. Y.; Chen, X. A novel electrochemiluminescence tetracyclines sensor based on a Ru(bpy)(2+)(3)-doped silica nanoparticles/Nafion film modified electrode. *Talanta* **2014,** *129*, 26-31.
14. Jalalian, S. H.; Karimabadi, N.; Ramezani, M.; Abnous, K.; Taghdisi, S. M. Electrochemical and optical aptamer-based sensors for detection of tetracyclines. *Trends Food Sci Tech* **2018,** *73*, 45-57.
15. Lin, T. R.; Li, Z. H.; Song, Z. P.; Chen, H.; Guo, L. Q.; Fu, F. F.; Wu, Z. J. Visual and colorimetric detection of p-aminophenol in environmental water and human urine samples based on anisotropic growth of Ag nanoshells on Au nanorods. *Talanta* **2016,** *148*, 62-68.

16. Wu, C.; Liu, Z.; Sun, H. H.; Wang, X.; Xu, P. Selective determination of phenols and aromatic amines based on horseradish peroxidase-nanoporous gold co-catalytic strategy. *Biosens Bioelectron* **2016,** *79*, 843-849.
17. Gan, T.; Wang, Z. K.; Wang, Y.; Li, X. Y.; Sun, J. Y.; Liu, Y. M. Flexible graphene oxide-wrapped SnO2 hollow spheres with high electrochemical sensing performance in simultaneous determination of 4-aminophenol and 4-chlorophenol. *Electrochim Acta* **2017,** *250*, 1-9.
18. Feier, B.; Gui, A.; Cristea, C.; Sandulescu, R. Electrochemical determination of cephalosporins using a bare boron-doped diamond electrode. *Anal Chim Acta* **2017,** *976*, 25-34.
19. Dizavandi, Z. R.; Aliakbar, A.; Sheykhan, M. A novel Pb-poly aminophenol glassy carbon electrode for determination of tetracycline by adsorptive differential pulse cathodic stripping voltammetry. *Electrochim Acta* **2017,** *227*, 345-356.
20. Devkota, L.; Nguyen, L. T.; Vu, T. T.; Piro, B. Electrochemical determination of tetracycline using AuNP-coated molecularly imprinted overoxidized polypyrrole sensing interface. *Electrochim Acta* **2018,** *270*, 535-542.
21. Gan, T.; Shi, Z. X.; Sun, J. Y.; Liu, Y. M. Simple and novel electrochemical sensor for the determination of tetracycline based on iron/zinc cations-exchanged montmorillonite catalyst. *Talanta* **2014,** *121*, 187-193.
22. Zhu, C.; Yang, G.; Li, H.; Du, D.; Lin, Y. Electrochemical sensors and biosensors based on nanomaterials and nanostructures. *Anal Chem* **2015,** *87* (1), 230-49.
23. Zhao, W. W.; Xu, J. J.; Chen, H. Y. Photoelectrochemical enzymatic biosensors. *Biosens Bioelectron* **2017,** *92*, 294-304.
24. Yang, Z. Q.; Wang, Y.; Zhang, D.; Chen, C. A sensitizing photoelectrochemical sensing platform strategy based on bio-etching preparation of Bi2S3/BiOCl p-n heterojunction. *Talanta* **2018,** *190*, 357-362.
25. Devadoss, A.; Sudhagar, P.; Terashima, C.; Nakata, K.; Fujishima, A. Photoelectrochemical biosensors: New insights into promising photoelectrodes and signal amplification strategies. *J Photoch Photobio C* **2015,** *24*, 43-63.
26. Zhao, W. W.; Xiong, M.; Li, X. R.; Xu, J. J.; Chen, H. Y. Photoelectrochemical bioanalysis: A mini review. *Electrochem Commun* **2014,** *38*, 40-43.
27. Wang, R.; Yan, K.; Wang, F.; Zhang, J. D. A highly sensitive photoelectrochemical sensor for 4-aminophenol based on CdS-graphene nanocomposites and molecularly imprinted polypyrrole. *Electrochim Acta* **2014,** *121*, 102-108.
28. Trashin, S.; Rahemi, V.; Ramji, K.; Neven, L.; Gorun, S. M.; De Wael, K. Singlet oxygen-based electrosensing by molecular photosensitizers. *Nat Commun* **2017,** *8*.
29. Schlothauer, J. C.; Hackbarth, S.; Jager, L.; Drobniewski, K.; Patel, H.; Gorun, S. M.; Roder, B. Time-resolved singlet oxygen luminescence detection under photodynamic therapy relevant conditions: comparison of ex vivo application of two photosensitizer formulations. *J Biomed Opt* **2012,** *17* (11).
30. Minnes, R.; Weitman, H.; Lee, H. J.; Gorun, S. M.; Ehrenberg, B. Enhanced acidity, photophysical properties and liposome binding of perfluoroalkylated phthalocyanines lacking C-H bonds. *Photochem Photobiol* **2006,** *82* (2), 593-9.
31. Beveridge, A. C.; Bench, B. A.; Gorun, S. M.; Diebold, G. J. Evaluation of photodynamic therapy agents through transient grating measurements. *J Phys Chem A* **2003,** *107* (25), 5138-5143.
32. Bench, B. A.; Beveridge, A.; Sharman, W. M.; Diebold, G. J.; van Lier, J. E.; Gorun, S. M. Introduction of bulky perfluoroalkyl groups at the periphery of zinc perfluorophthalocyanine: Chemical, structural, electronic, and preliminary photophysical and biological effects. *Angew Chem Int Edit* **2002,** *41* (5), 748-+.
33. Wilkinson, F.; Helman, W. P.; Helman, W. P. Rate Constants for the Decay and Reactions of the Lowest Electronically Excited Singlet State of Molecular Oxygen in Solution. An Expanded and Revised Compilation. *J Phys Chem Ref Data* **1995,** *24* (663).
34. Brown, K. C.; Corbett, J. F. Benzoquinone Imines .16. Oxidation of Para-Aminophenol in Aqueous-Solution. *J Chem Soc Perk T 2* **1979,** (3), 308-311.
35. Li, C.; Hoffman, M. Z. Oxidation of phenol by singlet oxygen photosensitized by the tris(2,2 '-bipyridine)ruthenium(II) ion. *J Phys Chem A* **2000,** *104* (25), 5998-6002.
36. Tratnyek, P. G.; Holgne, J. Oxidation of Substituted Phenols in the Environment - a Qsar Analysis of Rate Constants for Reaction with Singlet Oxygen. *Environ Sci Technol* **1991,** *25* (9), 1596-1604.
37. Moons, H.; Loas, A.; Gorun, S. M.; Van Doorslaer, S. Photoreduction and light-induced triplet-state formation in a single-site fluoroalkylated zinc phthalocyanine. *Dalton T* **2014,** *43* (40), 14942-14948.
38. Ribeiro, A. R.; Schmidt, T. C. Determination of acid dissociation constants (pK(a)) of. cephalosporin antibiotics: Computational and experimental approaches. *Chemosphere* **2017,** *169*, 524-533.
39. Zhao, C.; Pelaez, M.; Duan, X. D.; Deng, H. P.; O'Shea, K.; Fatta-Kassinos, D.; Dionysiou, D. D. Role of pH on photolytic and photocatalytic degradation of antibiotic oxytetracycline in aqueous solution under visible/solar light: Kinetics and mechanism studies. *Appl Catal B-Environ* **2013,** *134*, 83-92.
40. Gao, Y.; Li, Y.; Zhang, L.; Huang, H.; Hu, J. J.; Shah, S. M.; Su, X. G. Adsorption and removal of tetracycline antibiotics from aqueous solution by graphene oxide. *J Colloid Interf Sci* **2012,** *368*, 540-546.
41. Santos, L. H. M. L. M.; Paiga, P.; Araujo, A. N.; Pena, A.; Delerue-Matos, C.; Montenegro, M. C. B. S. M. Development of a simple analytical method for the simultaneous determination of paracetamol, paracetamol-glucuronide and p-aminophenol in river water. *J Chromatogr B* **2013,** *930*, 75-81.
42. Tsuji, A.; Nakashima, E.; Deguchi, Y.; Nishide, K.; Shimizu, T.; Horiuchi, S.; Ishikawa, K.; Yamana, T. Degradation Kinetics and Mechanism of Aminocephalosporins in Aqueous-Solution - Cefadroxil. *J Pharm Sci* **1981,** *70* (10), 1120-1128.
43. Fan, Y.; Liu, J. H.; Yang, C. P.; Yu, M.; Liu, P. Graphene-polyaniline composite film modified electrode for voltammetric determination of 4-aminophenol. *Sensor Actuat B-Chem* **2011,** *157* (2), 669-674.